J Electroceram (2007) 18:139–147
DOI 10.1007/s10832-007-9016-7

Defect chemistry of langasite III: Predictions of electrical and gravimetric properties and application to operation of high temperature crystal microbalance

Huankiat Seh · Holger Fritze · Harry L. Tuller

Received: 25 March 2006 / Accepted: 27 July 2006 / Published online: 16 February 2007

Abstract The electrical and gravimetric properties of langasite, $La_3Ga_5SiO_{14}$, are related to its underlying defect and transport processes via previously developed predictive defect and transport models. These models are used here to calculate the dependence of the partial ionic and electronic conductivities and the mass change for langasite as functions of temperature, dopant type and level and pO_2. Doping strategies devised for minimizing conductivity in langasite based on use conditions are described. For example, the required dopant level to achieve minimum conductivity and thus minimum electrical losses in acceptor-doped langasite is shown to depend on the operating pO_2. Likewise intrinsic mass changes in langasite, dependent on dopant level, pO_2 and temperatures, if high enough, can mask mass changes induced in active layers applied to langasite when used as a microbalance. For example, the model predicts that the dopant level in donor-doped langasite has less of an impact on intrinsic mass change due to external environmental changes when compared to acceptor-doped langasite. The models are also applied in defining acceptable operating limits needed to achieve and/or the design of properties for desired levels of microbalance resolution and sensitivity.

Keywords Resonator · Defect equilibria · Mixed ionic-electronic conductor

H. Seh (✉) · H. L. Tuller
Department of Materials Science and Engineering,
Massachusetts Institute of Technology,
Cambridge, MA 02139, USA
e-mail: huankiat@alum.mit.edu

H. Fritze
Department of Automation and Computer Science,
University of Applied Studies and Research,
38855 Wernigerode, Germany

1 Introduction

Langasite retains its piezoelectric properties up to its melting point of 1,470 °C and as such holds potential as a resonator platform for precision mass measurement and chemical sensor applications at high temperatures [1–4]. Surface acoustic wave (SAW) devices utilizing langasite have demonstrated operation to 750 °C [5, 6] and 1,000 °C [7], while bulk acoustic waves (BAW) devices have been operated to 1,400 °C [8].

By applying environmentally sensitive surface layers to langasite, high temperature resonant sensors can be developed. Specifically, adsorption or absorption of chemical species by the layers induces shifts in resonant frequency which may be correlated with mass changes and/or mechanical property changes. Likewise, such devices may be used as thin film deposition monitors, as commonly achieved today with the quartz crystal microbalance (QCM), but at elevated temperatures, allowing for in-situ deposition monitoring.

A typical BAW resonator consists of a single crystalline piezoelectric disk and a pair of key-hole shaped electrodes. An additional mass load can be applied as illustrated at the left of Fig. 1. In this work, langasite resonators are operated in the thickness shear mode for crystal cuts perpendicular to the y-axis as indicated at the right of Fig. 1.

The correlation between frequency shift, Δf_F, and mass uptake of a thin rigid foreign film, Δm_F, is given by the Sauerbrey Equation 1 [9]:

$$\Delta f_F / f_R = -\Delta m_F / m_R \quad (1)$$

where f_R and m_R are the resonance frequency and the mass of the unloaded resonator, respectively. Normally, this is adequate to explain the operation of a QCM, which typically operates at room temperature, where the mass of

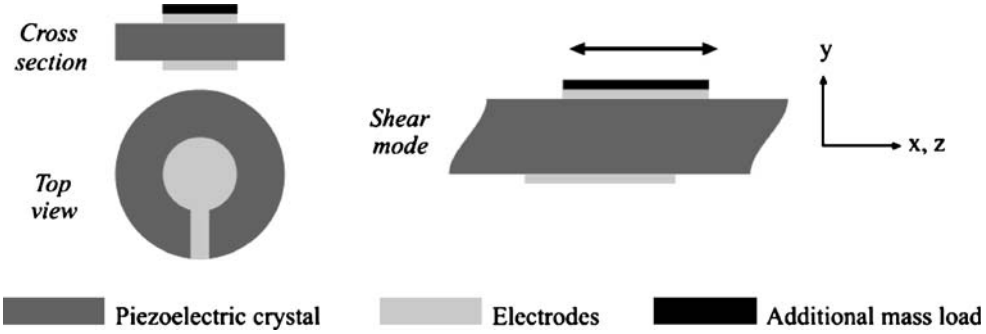

Fig. 1 Piezoelectric resonator showing shear mode operation

the quartz, m_R, remains unchanged with time. On the other hand, when the resonator is being operated at elevated temperature, the possible influence of operating conditions e.g., temperature and atmosphere, on the mass of the piezoelectric material (e.g., langasite) becomes important and requires a more sophisticated treatment than that of the Sauerbrey equation. The derivation of Eq. 2 is based on a one-dimensional physical model and reflects the influence of the density ρ_R, shear modulus c_R, piezoelectric constant e_R and dielectric constant ε_R on the resonance frequency [10]:

$$f_R = \frac{1}{2d_R}\sqrt{\frac{c_R - 8e_R^2/(\varepsilon_R\pi^2)}{\rho_R}} \tag{2}$$

Changes of the resonator material density or resonator mass ($\Delta m_\rho = A_R d_R \Delta\rho_R$) result in a frequency shift denoted by Δf_ρ:

$$\Delta f_\rho = -\frac{1}{4d_R}\sqrt{\frac{c_R - 8e_R^2/(\varepsilon_R\pi^2)}{\rho_R^3}}\Delta\rho_R$$

$$= -\frac{1}{4Ad_R^2}\sqrt{\frac{c_R - 8e_R^2/(\varepsilon_R\pi^2)}{\rho_R^3}}\Delta m_\rho \tag{3}$$

Here, the thickness and the effective area of the resonator are denoted by d_R and A_R, respectively. Similar to the Sauerbrey equation, the frequency shift can be related to a relative mass change:

$$\Delta f_\rho / f_R = \tfrac{1}{2}\Delta m_\rho / m_R \tag{4}$$

At sufficiently high temperature and/or extremes in pO_2, excessive reduction or oxidation of the langasite would result in sufficiently large changes in resonator mass Δm_ρ to interfere with the detection of mass changes Δm_F in the active films deposited onto the resonator, thereby effectively limiting its resolution. The prediction of how the resonator mass change Δm_ρ depends on temperature and gas atmosphere and the implication this has on the mass resolution of langasite resonators is a major objective of this paper. Changes induced in the shear modulus c_R, piezoelectric constant e_R and dielectric constant ε_R of langasite need also be taken into consideration but are beyond the scope of this paper.

At sufficiently elevated temperatures and certain ranges of oxygen partial pressure (pO_2), the resonant peak may become sufficiently broadened so as to negatively impact the resolution of the frequency measurement. The latter is strongly affected by the damping of the resonator which can be expressed by the resonator quality factor Q. Thereby, high losses correspond to low Q factors. Independent of particular models for the resonance behavior of the BAW resonators, Q can be calculated from the ratio of the resonance frequency f and the width w at half maximum of the admittance peak according to the right hand side of Eq. 5 [11]. Fitting the Lorentz function to the admittance peak, the resonance frequency follows from its maximum and the width at half maximum corresponds to its width. The lower part of Fig. 2 shows the resulting Q factor of langasite determined at temperatures up to 1,000 °C in air. Thereby, a network analyzer is used to acquire the resonance spectra in the vicinity of the resonance frequency. Simultaneously, the uncertainty of the resonance frequency is determined and expressed as its standard deviation σ. The upper part of Fig. 2 shows a clear increase in the uncertainty of the resonance frequency determination with temperature. The term 1.96 σ corresponds to a 95% probability of finding the frequency within the given values. A clear correlation between the loss expressed as the inverse resonator quality factor Q^{-1} and the uncertainty

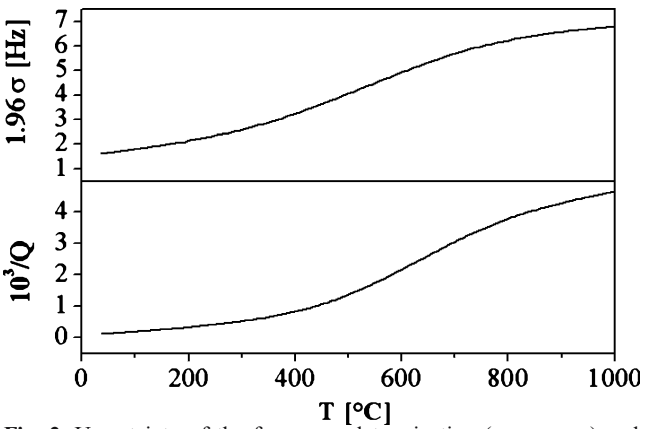

Fig. 2 Uncertainty of the frequency determination (*upper part*) and corresponding inverse resonator quality factor (*lower part*) of a 5 MHz langasite resonator as function of temperature

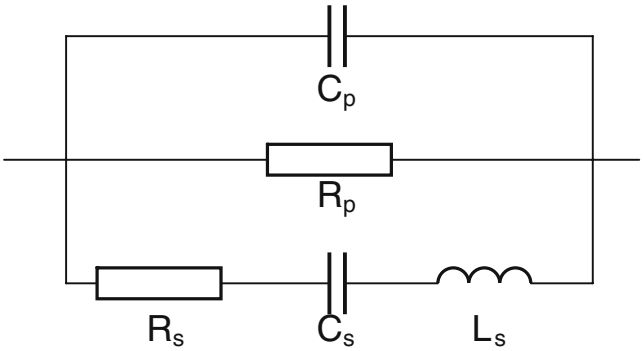

Fig. 3 Modified Butterworth–van Dyke equivalent circuit model with an additional R_p representing bulk resistance

in the peak frequency became obvious. Consequently, low losses or high quality factors are desirable to achieve accurate frequency measurements.

The increased associated electrical losses leading to performance degradation can be modeled using a modified Butterworth–van Dyke equivalent circuit model (Fig. 3). At high temperatures, the parallel resistive element R_p is added to represent the increased loss due to the lower bulk resistance of the resonator crystal and leads to the following expression for the quality factor [10]:

$$Q = \sqrt{\frac{L_s}{C_s}}\frac{1}{R_s}\frac{R_p}{R_p + R_s} = Q_0\frac{R_p}{R_p + R_s} \approx \frac{f}{w} \tag{5}$$

Here, Q_0 represents the quality factor at room temperature, i.e., for infinite values of R_p. The right hand side of the equation is already discussed above.

Since the quality factor, Q, has a direct dependence on R_p, the bulk resistance of the resonator, it must be controlled so that it remains sufficiently high. In this study, we examine means for decreasing the electrical conductivity and thus increase R_p via doping and control of temperature and oxygen partial pressure.

In order to engineer both the conductivity and the oxygen nonstoichiometry of langasite, we characterized its electrical properties under equilibrium conditions and determined its defect structure [12, 13]. In [12], acceptor doped langasite was shown to be a mixed ionic-electronic conductor with the ionic conducting specie being the oxygen vacancy fixed in concentration by the acceptor impurity. The electronic conductivity is dominated by electrons under reducing conditions for low acceptor levels and by holes under oxidizing conditions for higher acceptor levels with characteristic −1/4 and +1/4 power law dependences on pO_2, respectively. In [13], donor doped langasite was shown to be a predominantly electronic conductor via electrons. At high pO_2, the electron density is fixed by ionized donors; whereas at lower pO_2, electrons generated by reduction dominate with a characteristic −1/6 power law dependence on pO_2. Based on these studies, the oxidation and reduction equilibrium reactions were established and the mobilities of the major electrical carriers, i.e., oxygen vacancies, holes and electrons, were determined (see Table 1). The parameters listed in Table 1 provide means for predicting the bulk electrical conductivity and oxygen nonstoichiometry (i.e., mass change Δm_ρ) as functions of oxygen partial pressure, temperature and dopant concentration. The equilibrium constant K_r, K_o, K_e are defined in previous papers [12, 13] and are repeated here for convenience:

$$K_r = \left[V_o^{\bullet\bullet}\right] n^2 p O_2^{\frac{1}{2}} = k_r \exp\left(\frac{-E_r}{kT}\right), \tag{6}$$

associated with the reduction reaction,

$$O_O^X \rightarrow V_o^{\bullet\bullet} + 2e' + \tfrac{1}{2}O_2, \tag{7}$$

$$K_o = p^2\left[V_o^{\bullet\bullet}\right]^{-1} p O_2^{-\frac{1}{2}} = k_o \exp\left(\frac{-E_o}{kT}\right) \tag{8}$$

associated with the oxidation reaction,

$$\tfrac{1}{2}O_2 + V_o^{\bullet\bullet} \rightarrow O_o^x + 2h^{\bullet} \tag{9}$$

and,

$$K_e = np = k_e \exp\left(\frac{-E_g}{kT}\right), \tag{10}$$

associated with the electron-hole pair generation,

$$\text{null} \rightarrow h^{\bullet} + e'. \tag{11}$$

Note that distinct equilibrium constants K_r defining the reduction reaction are utilized for acceptor and donor doped langasite, respectively.

Table 1 Summary of langasite defect and transport model parameters.

	Acceptor-doped	Donor-doped
K_r $(cm^{-9}atm^{0.5})$	$K_r = 10^{67}\exp\left(-\frac{5.7\pm0.06eV}{kT}\right)$	$K_r = 10^{71}\exp\left(-\frac{6.57\pm0.24eV}{kT}\right)$
K_o $(cm^{-3}atm^{-0.5})$	$K_O = 4.6\times10^{18}\exp\left(-\frac{2.18\pm0.08eV}{kT}\right)$	N/A
K_e (cm^{-6})	$K_e = 6.8\times10^{42}\exp\left(-\frac{3.94\pm0.07eV}{kT}\right)$	N/A
Dopant Ionization	N/A	$[D^{\bullet}] = k_{Dn}^{1/2}\exp\left(-\frac{1.52\pm0.06eV}{2kT}\right)$
μ_e (cm^2/Vs)	N/A	$\mu_e = 1.1\times10^{-2}\exp\left(-\frac{0.15\pm0.01eV}{kT}\right)$
μ_h (cm^2/Vs)	$\mu_h = (4.9\pm0.1)T^{(0.096\pm0.002)}$	N/A
μ_{Vo} (cm^2/Vs)	$\mu_{Vo} = \frac{217}{T}\exp\left(-\frac{0.91\pm0.01eV}{kT}\right)$	N/A

2 Bulk conductivity prediction for langasite

2.1 Acceptor doped langasite

As acceptor doped langasite is a mixed ionic-electronic conductor, its total bulk conductivity is the sum of electronic and ionic conductivity:

$$\sigma_{\text{total}} = \sigma_{\text{ionic}} + \sigma_{\text{electronic}} \tag{12}$$

$$\sigma_{\text{total}} = 2q\left[V_o^{\bullet\bullet}\right]\mu_{Vo} + nq\mu_e + pq\mu_h \tag{13}$$

And since, for the acceptor-doped langasite, the Brouwer approximation $2\left[V_o^{\bullet\bullet}\right] \approx \left[A_c^{'}\right]$ can be applied, Eq. 13 can be written as [11]:

$$\sigma_{\text{total}} = q\mu_{Vo}[A'] + q\mu_e\sqrt{2}[A']^{-\frac{1}{2}}pO_2^{-\frac{1}{4}}K_r^{\frac{1}{2}} + q\mu_h\sqrt{\tfrac{1}{2}}[A']^{\frac{1}{2}}pO_2^{\frac{1}{4}}K_O^{\frac{1}{2}} \tag{14}$$

Using the parameters in Table 1, σ_{total} can be predicted as function of temperature, pO_2, and acceptor concentration. In all predictions, we assume no defect association or ordering (dilute solution approximation) nor cation nonstoichiometry given the generally excellent correlation obtained between theory and experiment. Discussion of possible acceptor-oxygen vacancy association is presented in [12] but does not influence the predictions presented here.

2.2 Donor doped langasite

The total conductivity of donor doped langasite, being predominantly electronic, is simply the *n*-type electronic conductivity:

$$\sigma = qn\mu_e \tag{15}$$

As derived previously in [13], the electron density for donor-doped langasite can be defined as:

$$n^3 - [Nb^{\bullet}]n^2 - 2K_r pO_2^{-\frac{1}{2}} = 0 \tag{16}$$

which can be solved to obtain a closed form solution for *n*. Using the parameters in Table 1, σ for donor doped langasite can be predicted as function of temperature, pO_2, and donor concentration.

2.3 Prediction of langasite conductivity; examples

The predictive model was built using the defect chemistry framework. Several examples are illustrated here to demonstrate the usefulness of the model in examining how the bulk conductivity can be minimized as a function of different variables (i.e., acceptor concentration, temperature, pO_2). Figure 4 illustrates the effect of acceptor concentration [A′] on the conductivity of langasite at 1,000 °C. Increased [A′] markedly depresses the *n*-type conductivity at low pO_2, while increasing the pO_2 independent ionic conductivity. Note that the effect of increased acceptor concentration is depressed conductivity at low pO_2, but at the expense of increased conductivity at high pO_2.

This is further illustrated in Fig. 5 which shows that the minimum conductivity (for minimizing electrical losses) for a given acceptor level depends on the operating pO_2. For example, if a langasite resonator is designed for operation in air, the lower the acceptor concentration, the lower the conductivity. However, if the operation is in a reducing environment, for example at log pO_2=−10, the minimum conductivity will be at ~10^{18} cm^{-3} acceptor level. Even higher acceptor levels would be needed to minimize the conductivity at log pO_2=−20.

Likewise, the conductivity of donor doped langasite was calculated at T=1,000 °C as a function of D for log pO_2=0, −10 and −20. These results are shown in Fig. 6. Here, one observes that minimum conductivity for langasite at pO_2= 1 atm is achieved by maintaining the donor concentration below 10^{17} cm^{-3}, where the conductivity remains reduction controlled; above 10^{17} cm^{-3} the conductivity becomes donor controlled. Indeed, at lower pO_2, where langasite becomes more strongly controlled by reduction, the donor concentration has little influence on the conductivity.

The predicted variation of langasite conductivity as function of dopant level (both acceptor and donor) is shown in Fig. 7. It is possible to infer that the lowest conductivity is obtained when langasite is intrinsic. However, to totally eliminate impurities from langasite, a large bandgap material, via dopant compensation will be difficult. Alternative doping strategies for langasite resonators operating at 800 °C can be devised based on Fig. 7. If a langasite resonator is to be used in the pO_2 range from 1 to 10^{-10} atm, a low

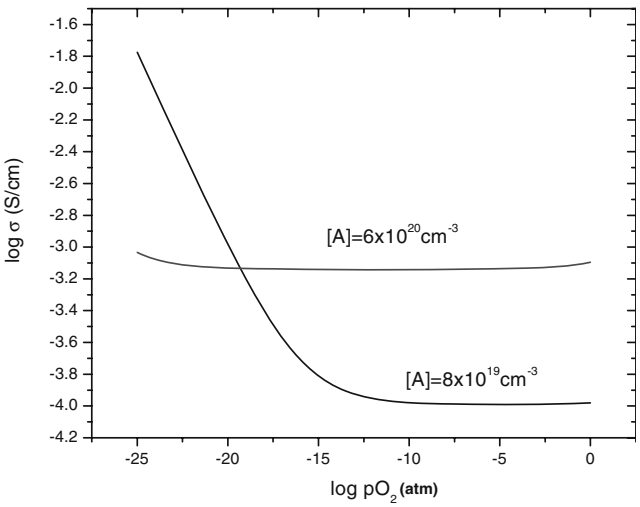

Fig. 4 Conductivity of acceptor doped langasite with [A′] equal to 6×10^{20} and 8×10^{19} cm^{-3} at 1,000 °C

concentration of donors will ensure a lower conductivity than using acceptor dopants. However, under strongly reducing environment (e.g., $pO_2=10^{-20}$ atm), low acceptor concentrations ensure a lower conductivity than do donor dopants.

The situation changes when the temperature is increased to 1,000 °C (Fig. 8). In air (pO_2 ~1 atm), a low concentration of donor dopant will allow for low conductivity. At a reducing environment ($pO_2=10^{-10}$ atm), a low acceptor dopant concentration will actually produce lower conductivity than donor doping. At extremely reducing environments ($pO_2=10^{-20}$ atm), the minimum conductivity is produced with an acceptor doping level of about 0.2%. This ability to incorporate operating conditions (i.e., temperatures and pO_2) together with doping considerations enables the design of langasite properties for improved operation performance (i.e., low electrical losses).

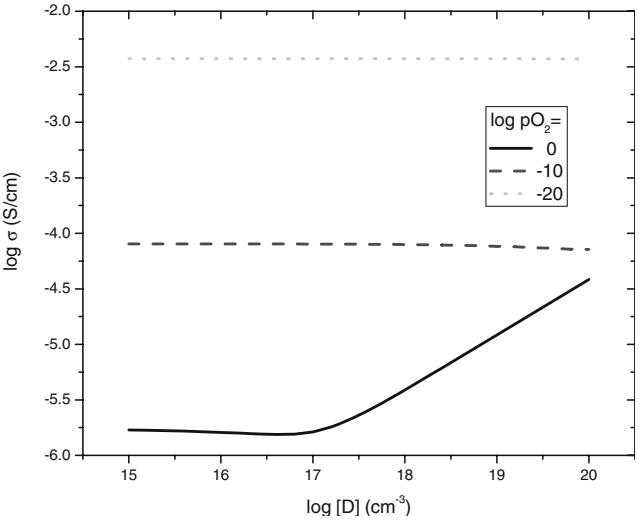

Fig. 6 Conductivity of donor doped langasite as function of donor concentration at 1,000 °C

3 Mass change prediction for langasite

The changing oxygen vacancy concentration with temperature or pO_2 results in a corresponding mass change in a langasite resonator, and, if significant, can mask the frequency shifts induced in the active layer designed to provide sensing. Predicting the mass change will assist in defining the resonator operating conditions for which oxidation and reduction processes will not interfere with the sensing process.

In the defect model for acceptor doped langasite, the Brouwer approximation was applied, fixing the oxygen vacancy concentration to the acceptor level $\left(2\left[V_O^{\bullet\bullet}\right] \approx [A']\right)$ in the ionic conduction regime. Nevertheless, reduction still occurs at those pO_2's as reflected in the generation of electrons with changing pO_2. The Brouwer approximation simply states that the generation of oxygen vacancies by redox processes is negligible compared to the total oxygen vacancy concentration formed in reaction to the acceptor doping. However, when considering changes in stoichiometry, as reflected in mass change, the oxygen vacancy creation accompanying the generation of electron has to be taken into account.

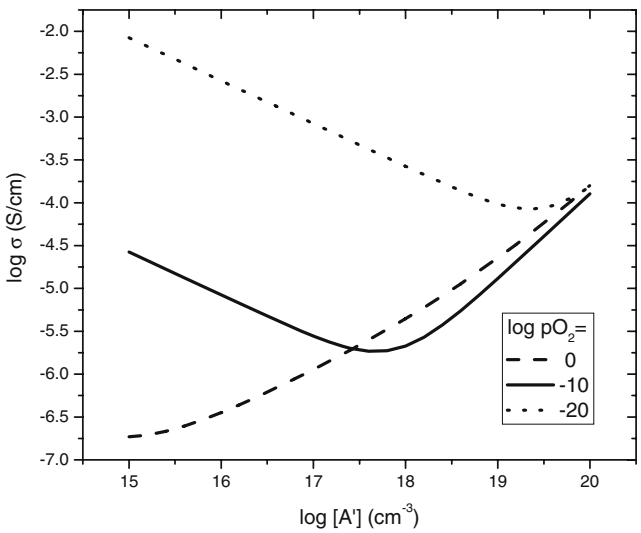

Fig. 5 Conductivity of acceptor doped langasite as function of acceptor concentration at 1,000 °C

The more complete neutrality condition for acceptor doped langasite is as follows:

$$n = 2\left[V_O^{\bullet\bullet}\right] - [A'] \tag{17}$$

Substituting Eq. 17 into the mass action law for reduction reaction gives:

$$\left[V_O^{\bullet\bullet}\right]^3 - \left[V_O^{\bullet\bullet}\right]^2 + \tfrac{1}{4}[A']^2\left[V_O^{\bullet\bullet}\right] - \tfrac{1}{4}pO_2^{-\frac{1}{2}}K_r = 0 \tag{18}$$

Using Eq. 18 and the K_r function listed in Table 1, the total oxygen vacancy concentration $\left[V_O^{\bullet\bullet}\right]$ can be calculated and n can then be determined as function of temperature, pO_2 and acceptor concentration with the assistance of Eq. 6. The change in oxygen vacancy concentration accompanying the generation of electrons is simply:

$$\Delta n = 2\Delta\left[V_O^{\bullet\bullet}\right] \tag{19}$$

The change in the vacancy concentration during operation (as temperature or pO_2 changes) can than be correlated to mass change.

In Fig. 9, the fractional mass change $\Delta m_\rho / m_R$ in langasite (normalizing to $pO_2=1$ atm) was predicted at 1,000 and 800 °C at three and one different acceptor dopant levels, respectively. The fractional mass change can be related to fractional frequency change using Eq. 4. For a bulk acoustic wave resonator fabricated from a 0.1% acceptor doped langasite operating at a typical resonant frequency of 10 MHz, a Δf of 16 Hz is expected if the

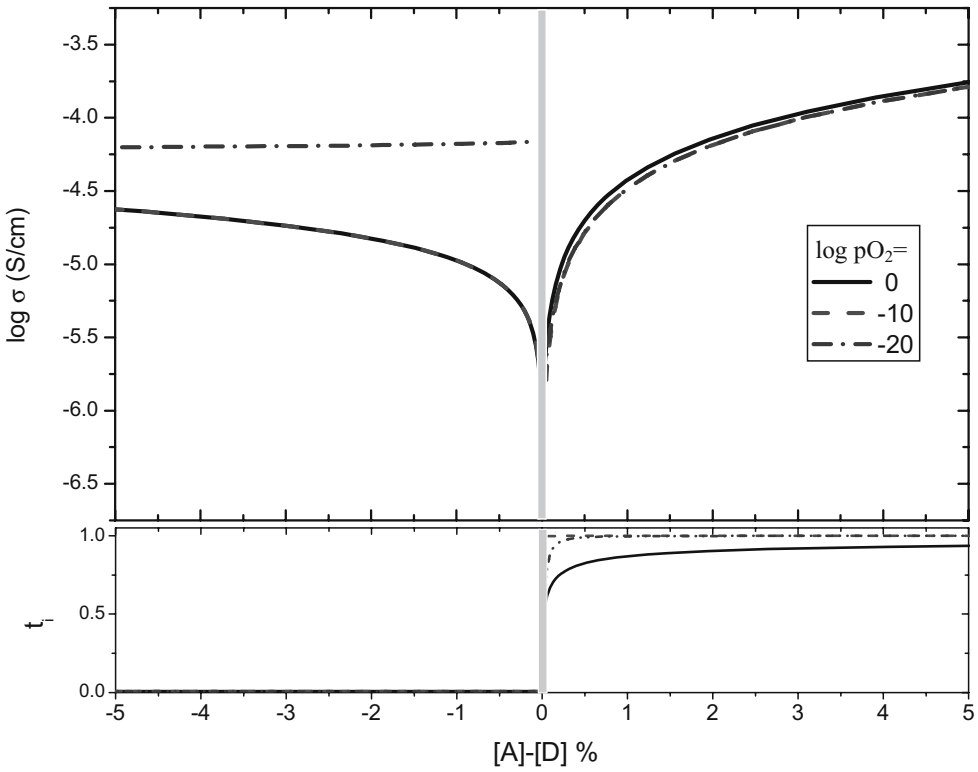

Fig. 7 Conductivity and ionic transport number prediction for langasite at three different pO_2 and 800 °C as function of dopant level

oxygen partial pressure changes from pO_2=1 atm to pO_2= 10^{-20} atm due to generation of oxygen vacancies ($1/2\ \Delta m/m = -\Delta f/f = -1.6 \times 10^{-6}$). This would limit the mass resolution of the resonator if it is to be used as a mass balance for investigating thin film oxygen stoichiometry which requires change in oxygen partial pressure of that magnitude, for example.

In Fig. 9, it can also be observed that the acceptor level has a small effect on the magnitude of mass change. Therefore, acceptor effects on both ionic and electronic

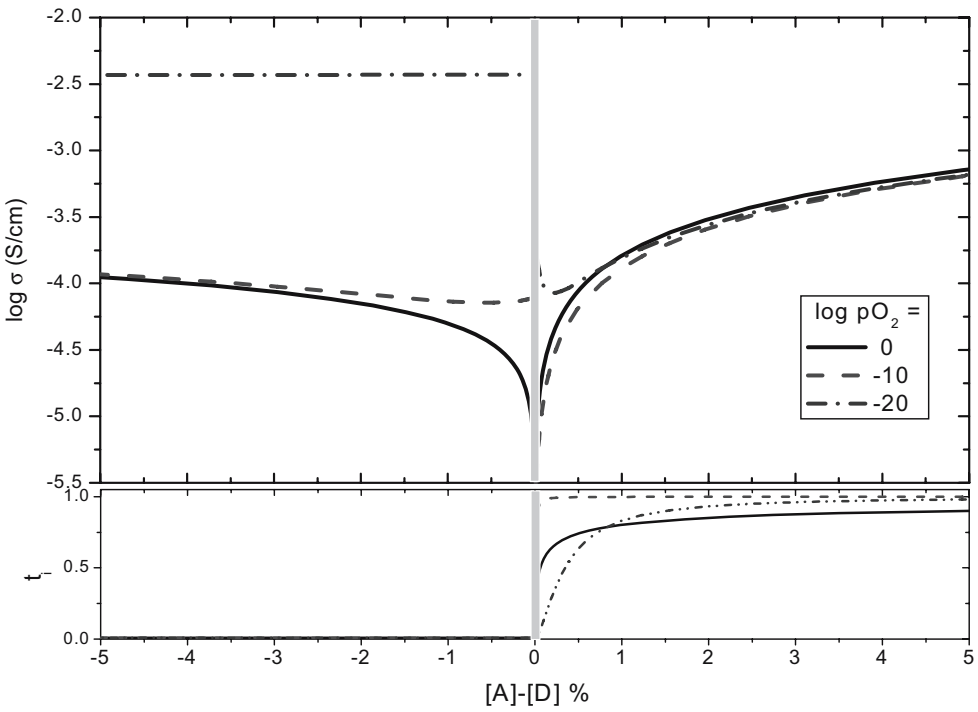

Fig. 8 Conductivity and ionic transport number prediction for langasite at three different pO_2 and 1,000 °C as function of dopant level

conductivity, which are considerably higher, will have larger impacts on the resolution and mass sensitivity limit of the resonator (i.e., from electrical losses).

The donor doped langasite is electronically compensated and the oxygen vacancy concentration varies with pO_2, either with −1/4 or −1/6 power law depending on the defect region. The mass change in donor doped langasite can be calculated using K_r (Table 1) and n (Eq. 17), which give oxygen vacancy concentration as function of temperature, donor level and pO_2. Figures 10 and 11 show the fractional mass change of three different donor doped langasite specimens at 1,000 °C as function of pO_2.

When compared to the acceptor case, it can be observed that donor concentration has an even smaller effect on the mass change (Fig. 11). For a bulk acoustic wave resonator fabricated from donor doped langasite operating at 10 MHz, Δf of 25 Hz is expected if the oxygen partial pressure changes from pO_2=1 atm to $pO_2=10^{-20}$ atm due to generation of oxygen vacancies ($1/2\ \Delta m/m = -\Delta f/f = -5 \times 10^{-6}$, regardless of the dopant level). The frequency change in this case is comparable to the acceptor doped case.

4 Impact of transport properties on resonator

With the ability to predict bulk conductivity and mass change in langasite as functions of temperature, dopant level and pO_2, it becomes possible to define the acceptable operating range (temperature and pO_2) for a langasite resonator, or to intentionally dope langasite for operation within specific conditions.

One way to define the operating requirements is to state an acceptable Q value from which the required R_p and hence the required conductivity can be calculated. Using an isoconductivity plot, for example, the desirable conditions can be defined. For example, Fig. 12 shows the isoconductivity lines of nominally undoped langasite (used in this work and in [15]). If the required conductivity is 10^{-4} S/cm or lower and the required pO_2 is ~10^{-15} atm, the operating temperature must be 950 °C or lower. In addition to electrical losses, significant mass change for nominally undoped langasite must be considered and could further restrict operating conditions.

The expression for Q can also be used for examining the influence of decreasing resonator resistance on Q. As temperature increases, R_p decreases while R_s increases. At high temperature (at approximately 900 °C or above for a 2 MHz Y-cut langasite crystal resonator studied previously [14, 15]), the values of R_p and R_s converge. At those temperatures, R_p becomes smaller than R_s, making Q proportional to R_p. Q is also inversely proportional to the half-height-width (HHW) of the spectrum obtained by the

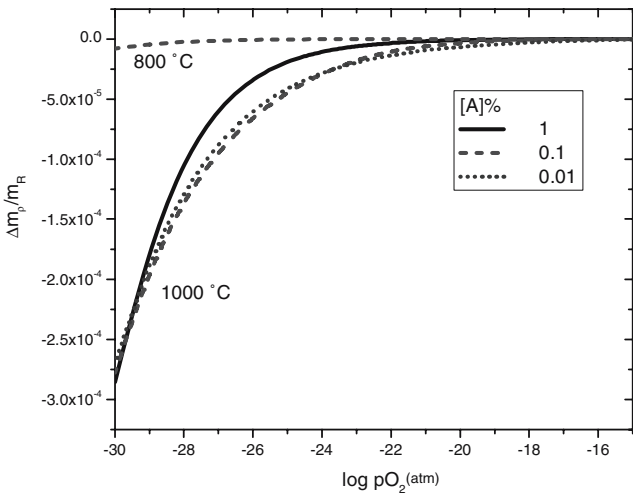

Fig. 9 Fractional mass change (relatively to langasite in air) in langasite with three acceptor levels at 1,000 °C and one acceptor level at 800 °C

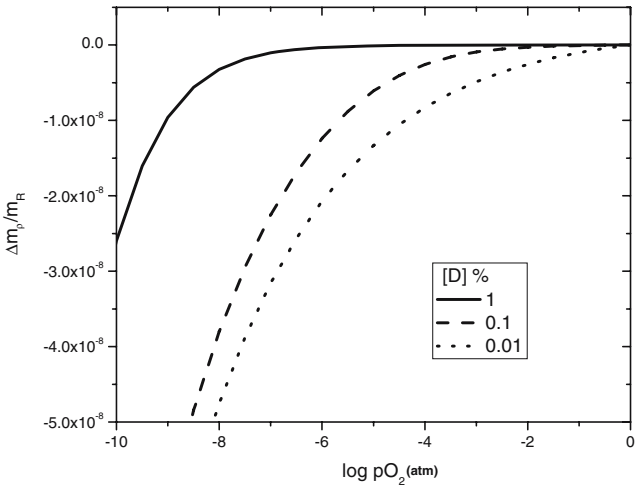

Fig. 10 Fractional mass change (relatively to langasite in air) in langasite with three donor levels at 1,000 °C (higher pO_2)

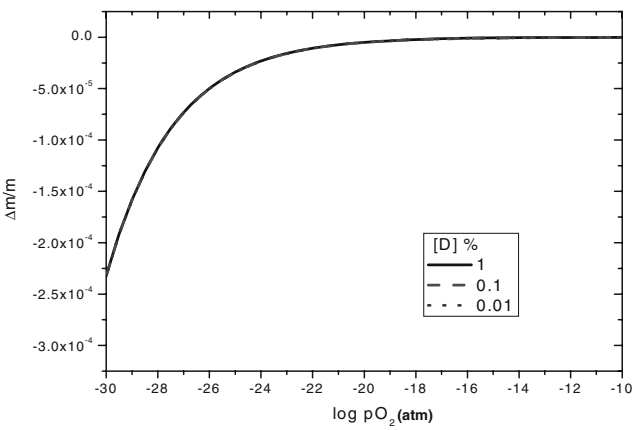

Fig. 11 Fractional mass change (relatively to langasite in air) in langasite with three donor levels at 1,000 °C (low pO_2). All three lines overlapped each other

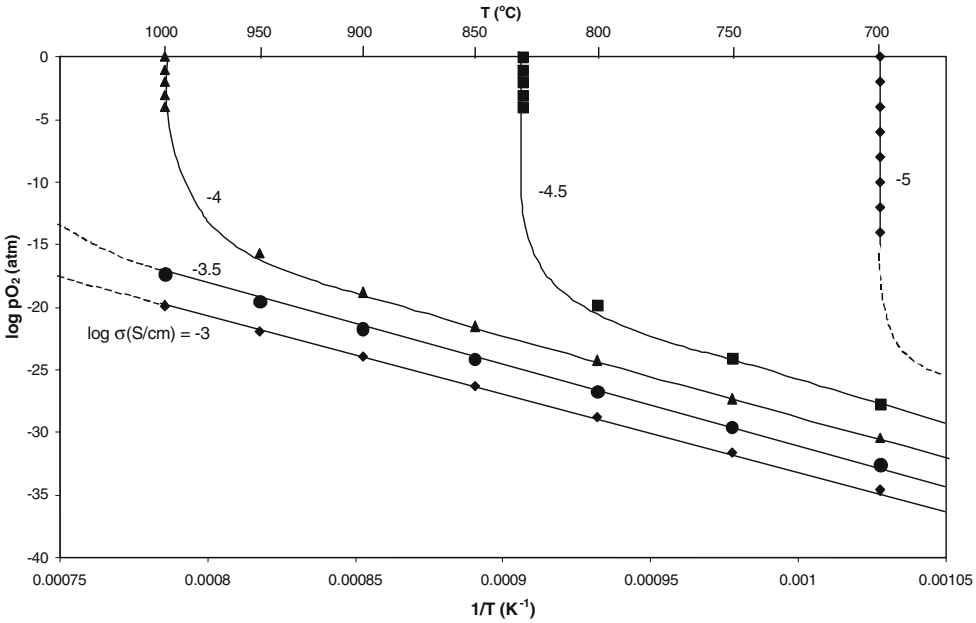

Fig. 12 Isoconductivity plot for nominally undoped langasite [15]

network analyzer, which can be equated to the uncertainty, δ, in resonant frequency of the resonator. Hence, R_p can be related and is inversely proportional to the uncertainty (δ). This relationship shows that increasing the conductivity by an order of magnitude (due to dopant or reduction/oxidation) can increase δ and thereby lower the sensitivity limit of the resonator by one order of magnitude at temperatures when electrical losses are high.

In fact, for the abovementioned 2 MHz Y-cut langasite crystal resonator (with electrode area of 0.43 cm^2 and assuming a 0.1% acceptor level), Q can be calculated as function of temperature and pO_2, and an iso-Q map can be derived (Fig. 13). This map gives us the operating limits of the resonator for a certain Q. For example, if Q is designed to be 1,000, the resonator must operate below 611 °C, whereas if Q must be greater than 100, the temperature must be kept below 850 and 775 °C for $pO_2=10^{-1}$ and 10^{-26} atm, respectively.

The fractional frequency change ($\Delta f/f$) due to change in oxygen vacancy concentration can also be related to the theoretical sensitivity limit for the resonator. The fractional frequency change caused by decreasing pO_2 by 20 orders of magnitude from pure oxygen at 1,000 °C is on the order of $\sim 10^{-6}$ (at 1,000 °C for both acceptor and donor doped langasite), which translates to ~10 Hz sensitivity limit in a 10 MHz langasite resonator. It has been stated above that, in theory, the frequency change would limit the resolution and sensitivity limit of the resonator. In practice, at high temperatures, the errors in resonant frequency measurements will be tens of hertz; the frequency change of a few

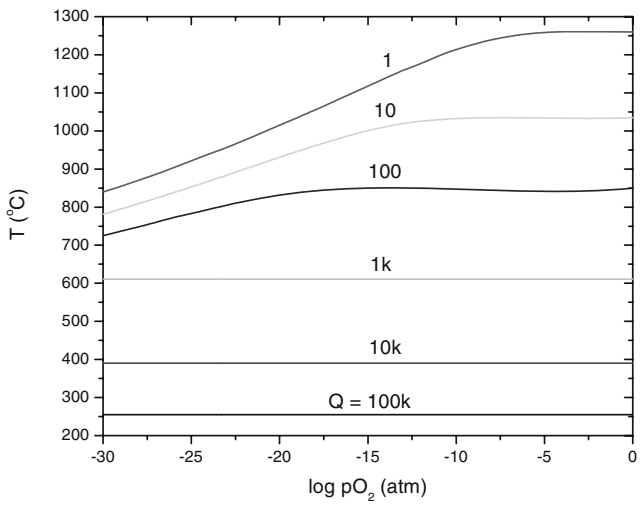

Fig. 13 Iso-Q map of 2 MHz langasite crystal (0.1% acceptor dopant) as function of temperature and pO_2

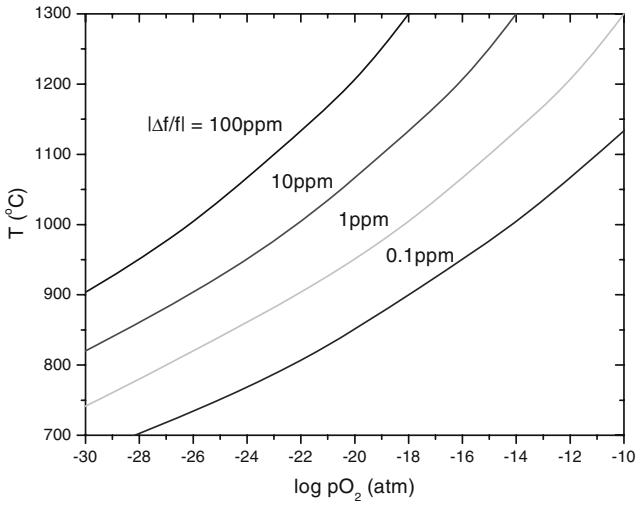

Fig. 14 Resolution limits of langasite resonator as function of temperature and pO_2

tens of hertz due to intrinsic mass change in langasite will play an insignificant role in limiting its resolution and sensitivity limit.

Figure 14 shows a map of resolution limit of langasite resonator. Since dopant levels play an insignificant role in the determination of $\Delta f/f$, this map can be used for all dopant levels to estimate the operation limits (i.e., the temperature and pO_2) of the langasite resonator. For example, if the required $\Delta f/f$ is 1 ppm (for around 10 Hz change due to oxygen non-stoichiometry in a 10 MHz crystal resonator), the operating condition must be below the 1 ppm line in Fig. 14.

5 Conclusion

The previously derived defect model was utilized in building a predictive model for langasite. This model was used to calculate the bulk electrical conductivity and mass change of langasite due to oxygen vacancy generation as functions of temperature, dopant level and pO_2. The establishment of defect specie concentrations and their mobilities as function of pO_2 and temperature allowed us to define the acceptable operating range and/or design the properties of langasite for minimum resistive loss and mass change, which affect the resolution and sensitivity limit of the resonator. At high temperature (900 °C or higher for 2 MHz langasite resonator), the electrical loss of langasite becomes significant. With the bulk resistance proportional to Q, this leads to increased uncertainty in the measurements, δ, of the resonator (i.e., lower resolution). On the other hand, it was also demonstrated that langasite exhibits only very small mass change due to oxygen stoichiometric change, and, even at 1,000 °C, $\Delta f/f$ is 2.5 ppm or less for a pO_2 change of as much as 20 decades.

Acknowledgement We would like to acknowledge National Science Foundation (NSF DMR-0228787, ECS-0428696 and INT-9910012), and the German Research Foundation (DFG) for providing support for this work.

References

1. B.V. Mill, Y.V. Pisarevsky, in *Langasite-type Materials: From Discovery to Present State*, IEEE/EIA International Frequency Control Symposium and Exhibition, 2000, pp. 133–144
2. R.C. Smythe, R.C. Helmbold, G.E. Hague, K.A. Snow, in *Langasite, Langanite and Langatate Resonators: Recent Results.* Joint Meeting EFTF-IEEE IFCS vol. 2 (1999), pp. 816–820
3. R.C. Smythe, R.C. Helmbold, G.E. Hague, K.A. Snow, IEEE Trans. Ultrason. Ferroelectr. Freq. Control **47**(2), 355–360 (2000)
4. R.C. Smythe, in *Material and Resonator Properties of Langasite and Langatate: A Progress Report*. IEEE International Frequency Control Symposium, 1998, pp. 761–765
5. J.A.Thiele, M.P.D. Cunha, in *High Temperature SAW Gas Sensor on Langasite.* IEEE Sensors, (IEEE, Toronto, Canada, 2003)
6. M.P.D. Cunha, J.A. Thiele. Electron. Lett. **39**(10), 818–819 (2003)
7. J. Hornsteiner, E. Born, G. Fischerauer, E. Riha, in *Surface Acoustic Wave* Sensors for High Temperature Applications. Proceeding IEEE Frequency Control Symposium, 1998, pp. 615–620
8. H. Fritze, J. Electroceram., **17**(2–4), 625–630 (2006)
9. G. Sauerbrey, Z. Phys. **155**, 206–222 (1959)
10. H. Fritze, O. Schneider, H. Seh, H.L. Tuller, G. Borchardt, Phys. Chem. Chem. Phys. **5**(23), 5207–5214 (2003)
11. W. Gopel, J. Hesse, J.N. Zehmel, *Sensors, A Comprehensive Survey.* (VCH, Weinheim, 1994), p. 211
12. H. Seh, H.L. Tuller, J. Electroceram. **16**:2, 115–125 (2006)
13. H. Seh, H.L. Tuller, J. Electroceram. **15**, 193–202 (2005)
14. H. Fritze, H.L. Tuller, H. Seh, G. Borchardt, Sens. Actuators, B **76**, 103–107 (2001)
15. H. Seh, H.L. Tuller, H. Fritze, Sens. Actuators B. **93**, 169–174 (2003)